Biophysical Journal
Article

Biophysical Society

$Venus_{A206}$ Dimers Behave Coherently at Room Temperature

Youngchan Kim,[1] Henry L. Puhl III,[1] Eefei Chen,[2] Grace H. Taumoefolau,[1] Tuan A. Nguyen,[1] David S. Kliger,[2] Paul S. Blank,[3] and Steven S. Vogel[1,*]

[1]Section on Cellular Biophotonics, National Institute on Alcohol Abuse and Alcoholism, National Institutes of Health, Bethesda, Maryland; [2]Chemistry and Biochemistry Department, University of California Santa Cruz, Santa Cruz, California; and [3]Section on Integrative Biophysics, Eunice Kennedy Shriver National Institute of Child Health and Human Development, National Institutes of Health, Bethesda, Maryland

ABSTRACT Fluorescent proteins (FPs) have revolutionized cell biology by allowing genetic tagging of specific proteins inside living cells. In conjunction with Förster's resonance energy transfer (FRET) measurements, FP-tagged proteins can be used to study protein-protein interactions and estimate distances between tagged proteins. FRET is mediated by weak Coulombic dipole-dipole coupling of donor and acceptor fluorophores that behave independently, with energy hopping discretely and incoherently between fluorophores. Stronger dipole-dipole coupling can mediate excitonic coupling in which excitation energy is distributed near instantaneously between coherently interacting excited states that behave as a single quantum entity. The interpretation of FP energy transfer measurements to estimate separation often assumes that donors and acceptors are very weakly coupled and therefore use a FRET mechanism. This assumption is considered reasonable as close fluorophore proximity, typically associated with strong excitonic coupling, is limited by the FP β-barrel structure. Furthermore, physiological temperatures promote rapid vibrational dephasing associated with a rapid decoherence of fluorophore-excited states. Recently, FP dephasing times that are 50 times slower than traditional organic fluorophores have been measured, raising the possibility that evolution has shaped FPs to allow stronger than expected coupling under physiological conditions. In this study, we test if excitonic coupling between FPs is possible at physiological temperatures. FRET and excitonic coupling can be distinguished by monitoring spectral changes associated with fluorophore dimerization. The weak coupling mediating FRET should not cause a change in fluorophore absorption, whereas strong excitonic coupling causes Davydov splitting. Circular dichroism spectroscopy revealed Davydov splitting when the yellow FP $Venus_{A206}$ dimerizes, and a novel approach combining photon antibunching and fluorescence correlation spectroscopy was used to confirm that the two fluorophores in a $Venus_{A206}$ homodimer behave as a single-photon emitter. We conclude that excitonic coupling between $Venus_{A206}$ fluorophores is possible at physiological temperatures.

INTRODUCTION

Both incoherent and coherent energy transfer (ET) between and within macromolecular assemblies are thought to play a fundamental role in biological systems, as exemplified in photosynthesis (1). Nonetheless, the role of quantum coherence in biological systems remains controversial because hot wet biological environments promote decoherence/dephasing (1,2). Even in photosynthesis, the role of long-lived quantum coherence has recently been questioned (3,4). ET between fluorophores can be mediated by Coulombic dipole-dipole coupling if donor and acceptor fluorophores share common atomic transitions (5). The coherence of ET, or lack of, is dictated by the relative rates of ET (K_{ET}, a function of fluorophore separation and orientation) and the rate of excited-state vibrational dephasing (2,6) ($K_{Dephasing}$, characteristically temperature dependent). Förster theorized three ET regimes based on coupling strength: "Very Weak" ($K_{ET} \ll K_{Dephasing}$), an intermediate "Weak" regime ($K_{ET} \approx K_{Dephasing}$), and "Strong" ($K_{ET} \gg K_{Dephasing}$) (7–9). In the very weak regime, fluorophores act independently, and energy transfers discretely from donors to acceptors via Förster's resonance ET (FRET) (5,7). At the other extreme in the strong coupling regime, donors and acceptors act as a single quantum entity because of the superposition of their excited states, with excitation energy distributed nearly instantaneously (5), and coherent ET (CET) prevails (1,5). Although Förster hypothesized that ET in the intermediate coupling regime should also be coherent (7), experimentally, little is known about this regime (10,11).

Submitted November 28, 2018, and accepted for publication April 16, 2019.

*Correspondence: stevevog@mail.nih.gov

Editor: Jochen Mueller.

https://doi.org/10.1016/j.bpj.2019.04.014

Compared to photosynthetic assemblies, fluorescent proteins (FPs), such as Venus (12), encase a single fluorophore within a β-barrel structure (13) and are easily modified by genetic engineering, making them amenable to studies of ET regimes. The diameter of the $Venus_{A206}$ β-barrel is $\geqq$2.2 nm, and its center-to-center fluorophore proximity in crystals is 2.5 nm, with a distance of closest approach of 1.5 nm (Fig. 1, *A* and *B*). Because the β-barrel limits the proximity of the adjacent FP fluorophores, coherent interactions between FPs is thought to be impossible. Accordingly, the extensive use of FPs for ET measurements (14) as a "spectroscopic ruler" (15) has been assumed to proceed by an incoherent FRET mechanism (5). Recently, Fleming's group measured a 2.2 ps anisotropy decay (corresponding to a 4.4 ps ET time constant) for ET between the fluorophores of dimeric yellow FP (YFP) (16). If the measured GFP dephasing time of ~1 ps (17) (~50 times slower than organic fluorophores (7)) is representative of other FP dephasing times, such as for YFP, the formalism of Knox and Kenkre (6,10) predicts that coherent FP intermediate-regime coupling may be possible.

Here, we describe room temperature experiments that investigate the following: 1) ultrafast ET between FPs when they dimerize (ultrafast here is defined as faster than the instrument response function of our time-resolved fluorescence anisotropy (TRFA) system, see Fig. S3)), 2) the appearance of Davydov splitting (18–20) (a quantum-mechanical spectral property of fluorophore coherence) associated with FP dimerization, and 3) the use of photon antibunching (AB) (21–23) with fluorescence correlation spectroscopy ((FCS) Fig. S2) (24–28) to confirm that excitonic coupling alters the independence of FP emission behavior.

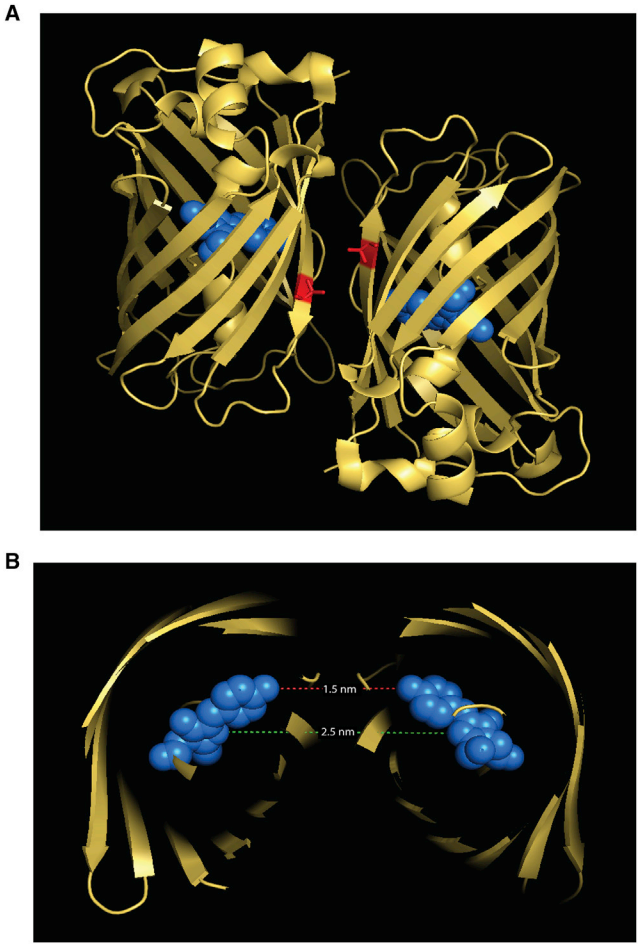

FIGURE 1 The crystal structure of $Venus_{A206}$ dimers. (*A*) Shown is an illustrated depiction of the structure of a pair of $Venus_{A206}$ molecules based on its crystal structure (12). Each Venus chromophore is depicted as blue spheres, and alanine-206, a residue involved in dimerization, is depicted in red. (*B*) A cut-away image of a $Venus_{A206}$ dimer revealing the separation between the two chromophores is shown. The dashed red line depicts the distance of closest approach, and the dashed green line illustrates the center-to-center distance.

MATERIALS AND METHODS

Molecular biology

$Venus_{A206}$ and $Venus_{A206K}$ purification

The 6His-tagged version of monomeric Venus ($Venus_{A206K}$) was constructed by cloning the $Venus_{A206K}$ open reading frame into a modified pRSETb vector (Thermo Fisher Scientific, Waltham, MA). The pRSETb vector was initially altered to incorporate an AgeI site after the 6His repeat: ATGCGGGGTTCTCATCATCATCATCATCATGGTGG**ACCGGT**CATGG CTAGCATGACTGGTGGACAGCAAATGGGTCGGGATCTGTACGAC GATGACGATAAGGATCCGAGCTCGAGATCTGCAGCTGGTACCATG GAATTCG**AAGCTT**GATC.

The mVenus ($Venus_{A206K}$) open reading frame was then cut from mVenus-C1 (a modified version of the Clontech vector YFP-C1) and cloned into the altered pRSETb vector using AgeI and *Hin*dIII.

The nonmonomeric version ($Venus_{A206}$) of 6His-tagged $Venus_{A206K}$ was generated by QuikChange Mutagenesis (Agilent Technologies, Santa Clara, CA) using the following primer and its reverse complement: CTACCTGAGCTACCAGTCC**GCC**CTGAGCAAAGACCCCAACG.

Both versions of Venus were purified using Nickel-NTA resin (QIAGEN, Hilden, Germany) from transformed BL21 (DE3) bacteria (New England BioLabs, Ipswich, MA). All incubations were performed at 37°C. Briefly, single colonies of transformed BL21 (DE3) bacteria were grown in Luria Bertani broth overnight under selection. Overnight cultures were diluted 1/30 with fresh antibiotic containing Luria Bertani and grown with shaking for 3–4 h. Isopropyl β-D-1-thiogalactopyranoside was added to 2 mM, and the cultures were shaken overnight. Bacteria were harvested by centrifugation (4000 rpm at 4°C). Pellets from ~1 L of culture were harvested for each construct and frozen at −80°C until the purification procedure. Pellets were thawed on ice, cleared *Escherichia coli* lysates were prepared under native conditions, and proteins were batch purified under native conditions as described in the QIAexpressionist manual (QIAGEN).

Purified protein was eluted with 250 mM imidazole and concentrated with Amicon Ultra Centrifugal filters (Millipore Ultracel-10 K) with a 10 kDa cutoff. Concentrated samples were stored at 4°C before use.

Absorbance spectra of purified $Venus_{A206}$ and $Venus_{A206K}$ fluorescence proteins were recorded on a NanoDrop One Microvolume Spectrophotometer (Thermo Fisher Scientific). Corresponding molar concentrations were calculated using Beer's law based on absorbance at 515 nm and an extinction coefficient of 126,000 $M^{-1}cm^{-1}$ for $Venus_{A206}$ and 127,000 $M^{-1}cm^{-1}$ for $Venus_{A206K}$ (29), respectively.

Venus$_{A206K}$-20nm-TD

mVenus-20nm-mVenus (Venus$_{A206K}$-20nm-TD) was constructed by inserting a synthetic oligonucleotide containing a codon-optimized version of a 20nm ER/K helix from *Trichomonas vaginalis* (30) into the previously described mVenus-17-mVenus (31). The oligonucleotide was optimized and synthesized (Thermo Fisher Scientific) with SalI ends and cloned into the SalI site of mVenus-17-mVenus (31): **GTCGAC**GAGGAAGAG GAAAAGAAGAAAGAGGAAGAAGAGAAGAAACAAAAAGAGGAA CAAGAACGGCTGGCCAAAGAGGAAGCCGAGCGCAAGCAGAAAG AAGAACAAGAGAGACTCGCCAAAGAAGAGGCTGAGAGGAAGCA AAAAGAAGAGGAAGAACGCAAACAAAAAGAAGAAGAGGAACG GAAGCAGAAAGAGGAAGAGGAACGAAAACTGAAAGAAGAACAA GAACGCAAGGCCGCCGAGGAAAAGAAAGCCAAAGAAGAAGCAG AGCGGAAAGCCAAAGAGGAACAAGAGAGAAAGGCCGAGGAAGA AAGAAAGAAAAAAGAGGAAGAGGAAAGGCTCGAGCGCGAGCGC AAAGAGCGCGAGGAACAAGAAAAGAAGGCTAAAGAGGAA**GTC GAC** and **VD**EEEEKKKEEEEKKQKEEQERLAKEEAERKQKEEQER LAKEEAERKQKEEEERKQKEEEERKQKEEEERKLKEEQERKAAEE KKAKEEAERKAKEEQERKAEEERKKKEEEERLERERKEREEQEKK AKEE**VD**.

Venus$_{A206}$-TD

The Venus-33-Venus dimer (Venus$_{A206}$-TD) was constructed as follows: a codon optimized version of monomeric Venus$_{A206K}$ (Vhp$_{A206K}$) was synthesized and cloned into the XbaI and ApaI sites of pcDNA3.1 (Thermo Fisher Scientific). Codon optimization incorporated enough degeneracy to allow PCR-based manipulations that are impaired by the redundancy of two identical Venus sequences. The NheI/*Hin*dIII Venus$_{A206K}$ fragment from mVenus-C1 was moved into the NheI/*Hin*dIII sites in front of the Vhp$_{A206K}$. The resulting 120 basepair linker was replaced by the following 99 basepair linker (33 amino acids), including a tobacco etch virus protease site (**ENLYFQG**): TCCGGACTCAGATCT**GAGAACCTG TACTTCCAGGGC**CCGCGGGAATTCTGCAGATATCCAGCACAGTG GCGGCCGCTCGAGTCTAGACCGCGGACCACC.

Sequential QuikChange Mutagenesis (Agilent Technologies) was used to convert the Venus$_{A206K}$ and Vhp$_{A206K}$ to nonmonomeric A206 forms. Primers for the Venus$_{A206K}$ to Venus$_{A206}$ were described above. Primers used for the A206 mutation in Vhp was the following and its complement: CTGAGCTACCAGAGC**GCC**CTGAGCAAGGACCC.

Cell culture, transfection, and homogenate preparation

HEK 293 cells (American Type Culture Collection, Manassas, VA) were grown as a monolayer in T-75 flasks (CytoOne) in a humidified incubator (Thermo Fisher Scientific) at 37°C with 9% CO_2 in Dulbecco's modified Eagle's medium (1×) plus GlutaMAX-1 media containing D-Glucose, sodium pyruvate, and 10% fetal bovine serum (Gibco, Gaithersburg, MD). HEK 293 cells were removed using TrypLE Express (Gibco by Life Technologies) and washed in Dulbecco's modified Eagle's medium and DPBS (without calcium or magnesium, Gibco by Life Technologies), respectively. After harvesting, cells were pelleted by centrifugation at 400 × *g* for 2 min, and the supernatant was discarded.

Transfections of plasmid DNA into HEK 293 cells were performed using the Neon Transfection System (100 μL kit; Thermo Fisher Scientific) and a microporation system (MicroPorator, Digital Bio/BTX, Shelton, CT). Plasmid DNA (typically 10 μg/300,000 cells) was added into a presterilized 1.6 mL microcentrifuge tube (Neptune Scientific, San Diego, CA) with cells. Transfected cells were cultured as a monolayer in 60-mm culture dishes (Corning, Corning, NY) and incubated overnight.

On the following day, transfected cells were rinsed with Dulbecco's phosphate-buffered saline (DPBS), harvested, and lysed using passive lysis buffer (Promega, Madison, WI). After a 10 min incubation at room temperature, homogenates were centrifuged at 23,897 × *g* at 4°C for 15 min to remove membrane and particulate matter. Supernatants were transferred to a 1.6 mL microcentrifuge tube and frozen at −20°C for storage. Supernatant aliquots were thawed on ice before experimental use and then appropriately diluted for TRFA, FCS, and photon AB measurements with DPBS (without calcium or magnesium, Gibco by Life Technologies) containing 0.2% Brij-35 Detergent (Thermo Fisher Scientific) to avoid aggregation. Clarified homogenates (typically 80 μL for TRFA, 150 μL for FCS measurements, and between 0.15 and 4 mL for photon AB) were loaded into glass-bottom dishes (P35G-1.5-7-C; MatTek, Ashland, MA) for analysis.

Time-correlated single-photon counting instrumentation

Schematics for the TRFA, FCS, and AB instrumentations are illustrated in Figs. S1 and S2. A mode locked Ti:Sapphire laser (Chameleon-Ultra II; Coherent, Santa Clara, CA) operating at a repetition rate of 80 MHz and tuned to a center wavelength of 950 nm was employed for two-photon excitation. The laser beam was first spatially filtered and expanded by a spatial filter assembly (KT310; Thorlabs, Newton, NJ) with a 25-μm diameter pinhole. The laser beam passed through a half-wave plate (AHWP10M-980; Thorlabs) and a near-infrared (IR) linear polarizer (LPNIR100-MP; Thorlabs) so that the power and polarization of the laser beam can be adjusted. The laser beam was guided onto a sample through the back port of an inverted microscope (Axio Observer D1; ZEISS, Oberkochen, Germany). A multiphoton short-pass dichroic beam splitter (FF670-SDi01-25636; Semrock, Rochester, NY) was used to reflect the excitation beam to a water immersion objective lens (C-Apochromat 63×/1.2 W Corr; ZEISS) that focused the beam to a diffraction-limited spot (~450 nm in diameter). Two-photon excited fluorescence from the sample could be collected by the same objective lens and spectrally filtered by transmitting through the same dichroic beam splitter. IR block (BG39; SCHOTT, Mainz, Germany) and band-pass filters (FF01-550/88-25; Semrock) located after the dichroic beam splitter were used to block any residual beam from the excitation laser. Two hybrid detectors (HPM-100-40; Becker & Hickl, Berlin, Germany) connected to a detector control module (DCC-100; Becker & Hickl) were used to detect fluorescence emission. Detected photons were processed with a time-correlated single-photon counting (TCSPC) module (SPC-150; Becker & Hickl) via a router (HRT-41; Becker & Hickl) at room temperature. SPCM software (Ver. 9.75; Becker & Hickl) running in FIFO mode for TRFA and FCS and in SING mode for photon AB was used for data acquisition.

For TRFA measurements, parallel- and perpendicular-polarized fluorescence was separated with a polarizing beam splitter augmented with linear polarizers and detected by dedicated hybrid detectors. For the TRFA measurements shown in Fig. 2, an additional neutral density filter located in front of the IR block filter was included to adjust two-photon excited fluorescence intensity from the sample at a high concentration.

For FCS and photon AB, a quarter-wave plate (AQWP10M-980; Thorlabs) was used to produce circular polarized excitation, and the polarizing beam splitter augmented with linear polarizers (see Fig. S1) was replaced with a nonpolarizing beam splitter.

A fast photodiode detector (DET10N; Thorlabs) was used in TRFA and FCS configurations to synchronize laser pulse excitation with data acquisition. In the photon AB configuration, one hybrid detector was used to synchronize the TCSPC card. A delay cable was used to connect the synchronization hybrid detector to the TCSPC card to allow the detection of photon coincidences with both positive and negative delay times.

Laser power (for two-photon excitation) was measured at the sample plane using a PM100D power meter (Thorlabs), and power was set to 10 mW for TRFA and 20 mW for photon AB and corresponding FCS measurements, unless otherwise stated. Acquisition times were 60 s for TRFA and FCS measurements and ranged between 5 min to 6 h for photon

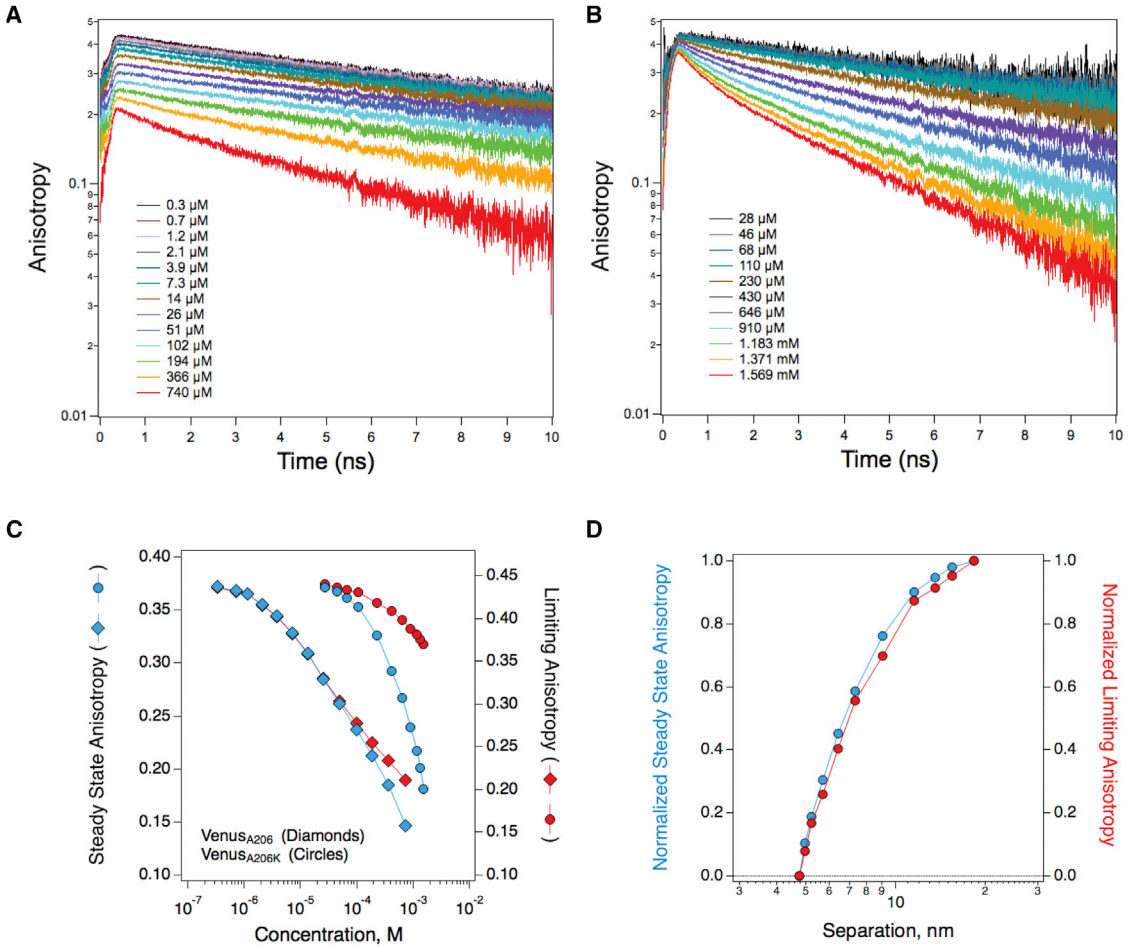

FIGURE 2 Ultrafast energy transfer between $Venus_{A206}$ dimers. The TRFA of $Venus_{A206}$ (*A*) and $Venus_{A206K}$ (*B*) is plotted for serial dilutions. (*C*) The limiting anisotropy *(red)* and steady-state anisotropy (*blue*) of $Venus_{A206}$ (*diamonds*) and $Venus_{A206K}$ (*circles*) were calculated from the time-resolved anisotropy decays depicted in (*A*) and (*B*) and are plotted as a function of concentration. (*D*) The normalized limiting anisotropy (*red*) and steady-state anisotropy (*blue*) of $Venus_{A206K}$ are plotted as a function of separation.

AB. Immersion fluid (Immersol W 2010; ZEISS) was used instead of water (with the water objective) to avoid evaporation during photon AB acquisitions. Sample volumes were 80 μL for TRFA measurements, 150 μL for photon AB and corresponding FCS measurements with acquisition times less than 30 min, and 4 mL for acquisition times longer than 30 min. Photon count rates were monitored before and after photon AB measurements to control for bleaching. A decrease in count rate was never observed under the experimental conditions described, arguing against significant levels of bleaching.

TRFA

TRFA, $r(t)$, was calculated using the following equation (32):

$$r(t) = \frac{I_{\parallel}(t) - g \cdot I_{\perp}(t)}{I_{\parallel}(t) + 2 \cdot g \cdot I_{\perp}(t)} \quad (1)$$

where $I_{\parallel}(t)$ and $I_{\perp}(t)$ are fluorescence intensity of parallel and perpendicular polarization components, and g is the instrument correction factor, which, for our system, had a value of 1.15 as determined by calibration using fluorescein tail fitting. Steady-state anisotropy, R, was calculated using the following equation:

$$R = \frac{\int I_{\parallel}(t) - g \cdot \int I_{\perp}(t)}{\int I_{\parallel}(t) + 2 \cdot g \cdot \int I_{\perp}(t)} \quad (2)$$

TRFA curves for $Venus_{A206}$ and $Venus_{A206K}$ at low concentrations were fit to a single exponential decay function to determine limiting anisotropies and rotational correlation times. At higher concentrations, a double exponential decay model was used to evaluate the limiting anisotropy.

$Venus_{A206K}$ concentration was converted to the average distance between molecules using the following equation (33):

$$D = \frac{0.55}{\sqrt[3]{C}} \quad (3)$$

where D is the average separation between fluorophores in solution (in nanometers), and C is the molar concentration.

Circular dichroism spectroscopy

Circular dichroism sample preparation

$Venus_{A206}$ and $Venus_{A206K}$ samples were prepared from their respective 280 μM stock solutions. The stock solutions were diluted with the

appropriate volumes of elution buffer (50 mM NaH_2PO_4, 300 mM NaCl, and 250 mM imidazole) at a pH of 8. To check sample integrity and concentration, absorption spectra were collected on an ultraviolet-visible spectrophotometer (V-750; JASCO, Easton, MD) before and after circular dichroism (CD) measurements.

Equilibrium CD experiments

Visible region (400–600 nm) CD spectra of 0.98, 14.5, and 280 μM $Venus_{A206}$ and $Venus_{A206K}$ were measured on a CD spectrophotometer (J-1500; JASCO). Protein and elution buffer spectra were collected using 10, 0.5, and 0.02 cm path length cuvettes, respectively. A total of 24, 16, and 27 spectra were collected for the three different $Venus_{A206}$ and $Venus_{A206K}$ samples that were prepared at each concentration. Data were collected every 0.1 nm with a 1 nm bandwidth using a digital integration time of 2 s and a scan speed of 20 nm/min. Absorption spectra were collected simultaneously on the CD spectrophotometer using the same parameters.

CD and absorption data analysis

CD and absorption data were processed using the JASCO Spectra Manager Spectra Analysis package. Difference CD spectra were obtained by subtracting the CD spectrum of $Venus_{A206}$ from that of $Venus_{A206K}$. Absorption peaks for $Venus_{A206K}$ and $Venus_{A206}$ at the different concentrations were determined using Gaussian fitting algorithms in SigmaPlot (v13.0) (SYSTAT Software).

Data analysis

IGOR Pro software was used to process and fit TRFA, FCS cross correlation, and photon AB data. GraphPad Prism 7 was used to calculate means, SD, analysis of variance, and Krustal-Wallis test with Dunn's multiple comparisons. Note, a reported SD value of 0.00 indicates an error smaller than 0.005. MacPyMOL (v1.7.4.2; Schrödinger) was used to represent the $Venus_{A206}$ dimeric structure for measuring fluorophore separation.

FCS

Typically, a single component three-dimensional Gaussian diffusion model (34) was used to fit the FCS cross correlation curve, as previously described (35–38):

$$G(\tau) = \frac{\gamma}{\langle N \rangle} \cdot \frac{1}{1 + (\tau/\tau_D)} \cdot \frac{1}{\sqrt{1 + (\omega/z)^2 (\tau/\tau_D)}} \quad (4)$$

where $<N>$ is the average number of fluctuating fluorescent molecules in the excitation/detection volume, τ_D is the correlation time (i.e., the average time a molecule spends in the excitation/detection volume), τ represents the lag time, and ω and z are the radial and axial beam waists, respectively, and γ, a volume shape factor, is assumed to have a value of 0.35. Lifetime normalized brightness was measured by auto-fluorescence polarization and fluctuation analysis, as previously described (38).

The average number of fluctuating fluorescent molecules, <N>, in Eq. 4 is the product of the average concentration, <C>, and the observation volume, V. Both γ and V will change with two-photon excitation power. Because of uncertainties in the experimental values of both γ and V in FCS measurements, Eq. 4 was redefined to consolidate this uncertainty into a single term for FCS measurements that correlated with AB (39):

$$G(\tau) = \frac{\chi_\gamma}{\langle C \rangle} \cdot \frac{1}{1 + (\tau/\tau_D)} \cdot \frac{1}{\sqrt{1 + (\omega/z)^2 (\tau/\tau_D)}} \quad (5)$$

where $\chi_\gamma = \gamma/V$. Theoretically, χ_γ can have values ranging between 0 and 1 (39). In this study, χ_γ was set to a value of 1 because with 20 mW excitation power for AB (approaching saturation), this value produced C/S versus $1/G_{(0)}$ plots in good agreement with photon AB Monte-Carlo simulations (Fig. 4).

Photon AB

Photon AB coincidence curves (for five-laser pulses) were fit using the following equation (23) modified for fitting a center peak flanked by two side peaks on each side:

$$A + C\ exp\left(-\frac{|t|}{\tau}\right) + S\sum_{\substack{j=-2 \\ j\neq 0}}^{j=2} exp\left(-\frac{|t - j \cdot T_{rep}|}{\tau}\right) \quad (6)$$

where A is the background noise, t is time, C is the amplitude of the center peak coincidences at $t = 0$, S is the average amplitude of the four-flanking side peak coincidences (at $j = -2$, -1, 1, and 2), τ is the fluorescence lifetime of the fluorophore, and T_{rep} is the time period between subsequent laser pulses. Once measured by fluorescence lifetime and time-resolved anisotropy measurements, τ and T_{rep} values were fixed for fitting subsequent photon AB curves.

AB Monte-Carlo simulations of a Hanbury-Brown- and Twiss (40)-based experimental AB setup using a pulsed laser for excitation, a soluble fluorophore as a sample, and a TCSPC card for detecting coincidences were performed using IGOR Pro software (v 8). Inputs into the simulation included <N>, the average number of fluorescent molecules in the observation volume (having a value ranging from 0.5 to 10), τ, the lifetime of the fluorophore (set to 3 ns), the laser repetition rate (set to 12.5 ns), and the molecular signal-to-noise ratio (S/N), defined as the probability of detecting an emitted photon per laser pulse (per fluorophore molecule present) divided by the probability of detecting a noise signal per laser pulse. The molecular S/N was set to 10, but because the AB fitting Eq. 6 controls for noise through parameter A, Monte-Carlo simulations C/S measurements yielded similar results when the S/N values ranged from 2 to 100 (data not shown). For each AB curve simulation at a specific <N> value, 20,000 photon coincidences were generated. A single simulated coincidence involved generating a trigger photon (that could potentially arise from either signal or noise at their relative probabilities of detection) that triggers our simulated TCSPC card, and a stop photon to simulate the stop signal in a TCSPC card. The stop signal is generated as a function of the five-laser pulses in the simulation (again arising from either signal or noise). The first photon detected in the five-pulse sequence, potentially caused by either signal or noise, was used as the simulated stop signal. For each coincidence generated, a Δ time value was calculated by subtracting the trigger time from the stop time. In each of the 20,000 coincidences generated per measurement, <N> was used as an input for a stochastic Poisson-based random number generator (PoissonNoise) to stochastically determine how many fluorescent molecules (N) were present in the observation volume at any individual trial. Each fluorophore present in the observation volume had an equal probability (always $\leq$0.01) to yield a detected photon as a result of each of the five-laser excitation pulsed simulated. In the third laser pulse (corresponding to Δ time = 0) of a sequence, N was set to N $-$ 1 to simulate AB. The variable τ was used as an input to a stochastic exponential random number generator (expNoise) to determine the time a signal photon was detected relative to the time of that specific laser pulse in the five-pulse sequence. Noise signals were generated by a stochastic white noise random number generator (eNoise) that had an equal probability for detection at any time during the five-laser pulse sequence. In the TCSPC setup used for AB measurements in this study, the first photon detected in a five-pulse sequence precludes subsequent photons from being detected (because of the instrumental dead time of $\sim$100 ns). Thus, this method for measuring

coincidences will have a pulse number bias if the probability of detecting a photon per laser pulse is high. To avoid this bias in the simulation, as mentioned above, photon detection probability per laser pulse was always low (1%), and the probability for detecting a noise count at an S/N of 10 was 0.1%. For comparison, in the actual AB experiments reported here, the photon detection probability per laser pulse was <0.2%. This value was not used in the Monte-Carlo simulation because it required excessive computational times and because control experiments indicated that at a simulated photon detection probability per laser pulse of 1% laser pulse, bias was no longer observed.

Derivation of closed form solution for the C/S ratio in the solution as a function of <N>

Let N be the number of molecules present in an "ideal" excitation volume. Each molecule has exactly one emitter. Thus, the number of molecules equals the number of emitters. Experimentally, the number of molecules, N, is obtained from the intensity autocorrelation functions at $\tau = 0$ ($G_{(0)}$ ~1/N, where a multiplicative geometry and excitation factor is required for equality). The number of emitters in the same excitation volume can be obtained from an AB experiment, often evaluated by comparing the ratio of the center (C) to side (S) peaks (R = C/S) in a pulsed TCSPC type of experiment. In a deterministic formulation, R = 1 − 1/N; R = 0 for one molecule having one emitter, R = 0.5 for two molecules, and R = 0.667 for three molecules. Deterministic R does not consider the probability distribution of N. The problem is how to fit the parametric data set that compares R with N for values of <N> and <R> obtained experimentally using AB and FCS from the same samples.

The deterministic formulation has R(N) = 1 − 1/N, exactly. However, we can consider the average <R(N)> by postulating a probability mass function. The first choice is the Poisson distribution. However, the probability mass function of the Poisson distribution includes N = 0, which is an undefined value of R(N). Because an N = 0 situation contributes no molecule derived co-incidents, consider the zero-truncated Poisson (ZTP) distribution instead:

$$ZTP = g(N, \langle N \rangle) = P(X = N | X>0) = \frac{\langle N \rangle^N}{(e^{\langle N \rangle} - 1) \cdot N!}; \; N = 1, 2, 3, \ldots \quad (7)$$

Using the ZTP, we calculate the expected or average value of R(N) as the following:

$$\begin{aligned} \langle R \rangle &= \sum_1^\infty \left(1 - \frac{1}{N}\right) \cdot \frac{\langle N \rangle^N}{(e^{\langle N \rangle} - 1) \cdot N!} \\ &= 1 - \sum_1^\infty \frac{\langle N \rangle^N}{(e^{\langle N \rangle} - 1) \cdot N \cdot N!} \\ &= 1 - \frac{1}{(e^{\langle N \rangle} - 1)} \cdot \sum_1^\infty \frac{\langle N \rangle^N}{N \cdot N!}. \end{aligned} \quad (8)$$

Although calculations can be done using the summation, a closed form of the summation exists, and can be used instead.

An analytic expression for the summation is the following:

$$\sum_1^\infty \frac{\langle N \rangle^N}{N \cdot N!} = (Ei(\langle N \rangle) - \ln(\langle N \rangle) - \gamma) \quad (9)$$

where $Ei(<N>)$ is the exponential integral, ln is the natural logarithm, and γ is the Euler-Mascheroni Constant (~0.57721566490). The model for the average center/side ratio, in terms of the ZTP parameter $<N>$, is:

$$\langle R \rangle = 1 - \frac{(Ei(\langle N \rangle) - \ln(\langle N \rangle) - \gamma)}{(e^{\langle N \rangle} - 1)} \quad (10)$$

Note, although we associate $<N>$ with the average number of molecules in the excitation volume, in fact, the ZTP expected value of X and the variance of X in terms of the $<N>$ parameter differs from $E(X) = <X>$ and $Var(X) = <X>$, which are the relationships for a pure Poisson-distributed variable.

RESULTS

$Venus_{A206}$, like its progenitor YFP_{A206} (41), dimerizes (Fig. 1) at concentrations approaching its dissociation constant (42), whereas the genetically modified $Venus_{A206K}$ (13) remains monomeric. Because TRFA measures molecular rotation and ET (32,43), we used it to determine at what concentration $Venus_{A206}$ dimerizes (Fig. 2, *A* and *B*). At low concentrations (1.2 and 28 μM, respectively) the fluorescence anisotropy decays (32) of both $Venus_{A206}$ and $Venus_{A206K}$ were described by a single exponential decay model and yielded similar rotational correlation times (16.6 ± 0.0 and 16.7 ± 0.1 ns, mean ± SD), in good agreement with the published monomeric Venus value (44), and both had identical limiting anisotropies (the anisotropy immediately after excitation and presumably before ET or molecular rotation, $R_0 = 0.43 \pm 0.00$). We conclude that at low concentrations, they are both monomeric.

Because chromophore separation in $Venus_{A206}$ dimers is ~2.5 nm, FRET theory (45–47) predicts a ~34 ps ET rate constant (using $R_0 = 5.3$ nm (48), $\tau_D = 3.1$ ns (44)), assuming that κ^2, the dipole orientation factor (49–51), is 2/3. Even faster ET can be expected (5.7 ps) if κ^2 is assumed to be 4. For homo-FRET between fluorophores in a dimer measured using TRFA, this corresponds to an anisotropy decay constant of ~17 and 2.85 ps, respectively (32). Thus, even in the incoherent very weak coupling regime an ultrafast ET-associated anisotropy decay component should appear as dimers form. Furthermore, if this component decays faster than the instrument response function (Fig. S3), as expected, it should manifest as an instantaneous drop in the limiting anisotropy whose amplitude is inversely proportional to the fraction of dimers in the population and which decreases with the concentration. As expected, a progressive and comparable decrease in both steady-state and limiting anisotropies was observed as the $Venus_{A206}$ concentration increased from 4 to 100 μM (Fig. 2, *A* and *C*). Above 100 μM, steady-state and limiting anisotropies diverged (Fig. 2 *C*), suggesting that homo-FRET between $Venus_{A206}$ dimers in close proximity (<10 nm) can also contribute to depolarization.

Because $Venus_{A206K}$ is thought to be monomeric, ET should only occur when separations fall below the critical distance required for homo-FRET (assuming that the dipole orientation factor, κ, is permissive for ET, i.e., $\kappa \neq 0$). Because the mean distance between monomers decreases

as the concentration increases (33), when the critical distance is attained, additional anisotropy decay components should appear (32). As expected, at concentrations above 100 μM, ET manifested as a progressive drop in steady-state and limiting anisotropy (Fig. 2, *B* and *C*), with a common dependence on distance (Fig. 2 *D*).

It is important to note that other factors can potentially modulate the drop in limiting anisotropy that we interpret as ultrafast ET. These include the numerical aperture of the microscope objective used (52,53), the excitation laser pulse repetition rate, and the excitation laser wavelength. Control experiments were performed to characterize their impact on our anisotropy measurements. Excitation wavelength (Fig. S4) and laser pulse rate (Fig. S5) had virtually no influence on the relative magnitude of the drop in limiting anisotropy we observe. In contrast, the use of a high numerical aperture objective may result in a small underestimation of the true magnitude in the drop in the limiting anisotropy (Fig. S6).

CD spectroscopy can be used to identify coherent $Venus_{A206}$ interactions associated with intermediate or strong coupling (9,19). Davydov splitting (18,19) results from a quantum superposition of coherently interacting components corresponding to in phase and out of phase combinations of fluorophore excited states. Because these components have an opposite rotational strength, their sum can be observed as a distinctive bisignate CD couplet. CD spectra from matched $Venus_{A206}$ and $Venus_{A206K}$ samples were measured at three different concentrations (Fig. 3). At low concentrations, in which both are monomeric, their CD spectra were indistinguishable (Fig. 3 *A*) and resembled the spectrum of YFP (54). At higher concentrations, the $Venus_{A206}$ CD spectrum changed progressively. Between 460 and 516 nm, the amplitude increased, whereas between 516 and 540 nm, it decreased with a minimum at 522 nm. At high concentrations, the CD spectrum was reminiscent of tetrameric DsRed (54). In contrast, the $Venus_{A206K}$ CD spectrum did not change with the concentration. Difference CD spectra revealed a couplet with Davydov splitting of 14.6 $\pm$ 0.3 nm (mean $\pm$ SD, n = 3) and a crossover point centered at ~516 nm (Fig. 3 *B*). By comparing the peak absorption wavelength at low and high concentrations (data not shown), a red shift in the $Venus_{A206}$ absorption spectrum was observed (515.9 $\pm$ 0.3, n = 24; 516.8 $\pm$ 0.3 nm, n = 27; mean $\pm$ SD; $p <$ 0.0001, Krustal-Wallis test with Dunn's multiple comparisons), whereas at low concentrations, the $Venus_{A206}$ and $Venus_{A206K}$ absorption peaks were identical ($p > 0.9999$). We conclude that coherent interactions can occur between paired $Venus_{A206}$ fluorophores.

If paired $Venus_{A206}$ fluorophores interact coherently, they should behave as a single quantum entity and therefore only be able to emit one photon at a time. To determine if coherent interactions alter $Venus_{A206}$ quantal behavior, we developed a method, AB/FCS fingerprinting, based on

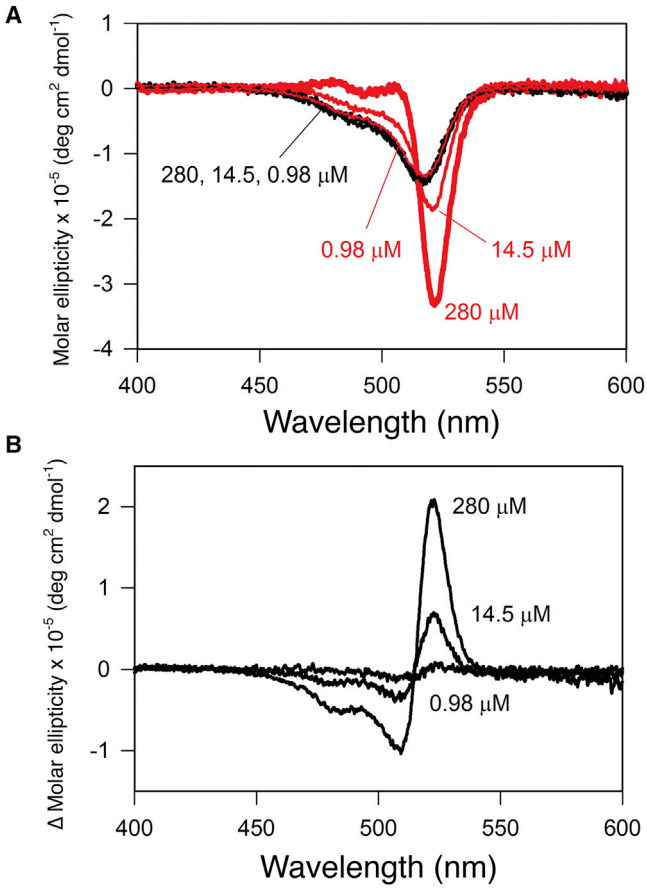

FIGURE 3 Dimerization alters the $Venus_{A206}$ CD spectrum. (*A*) The CD spectra of $Venus_{A206}$ (*red*) and $Venus_{A206K}$ (*black*) were measured at low (0.98 μM), intermediate (14.5 μM), and high (280 μM) concentrations. (*B*) To visualize Davydov splitting, the difference CD spectrum for each fluorophore concentration was calculated from the data presented in (*A*) by subtracting the $Venus_{A206}$ CD spectrum from its matching $Venus_{A206K}$ CD spectrum.

photon AB (21) and FCS (27,55). AB/FCS fingerprinting compares the number of independent emitters and fluorescent molecules in the same sample (Fig. 4). We built a microscope that can be rapidly reconfigured to measure either FCS or photon AB from serial dilutions of a fluorescent sample (Fig. S2). FCS monitors fluctuations in the intensity of emissions from a sample (56–59), and cross correlation of these fluctuations yields a correlation curve as a function of time, $G_{(\tau)}$ (Fig. 4). As time approaches zero, the curve asymptotically approaches a value called $G_{(0)}$, which is inversely proportional to the average number of fluctuating fluorescent molecules in the excitation/detection volume (26,34,59,60). Photon AB plots a histogram of the number of coincident photons detected with a corresponding Δ time value (the time difference between when a photon was detected by each detector). This plot is proportional to the probability of detecting two coincident photons with the corresponding Δ time, and at the center peak, this probability will be a function of the number of independent

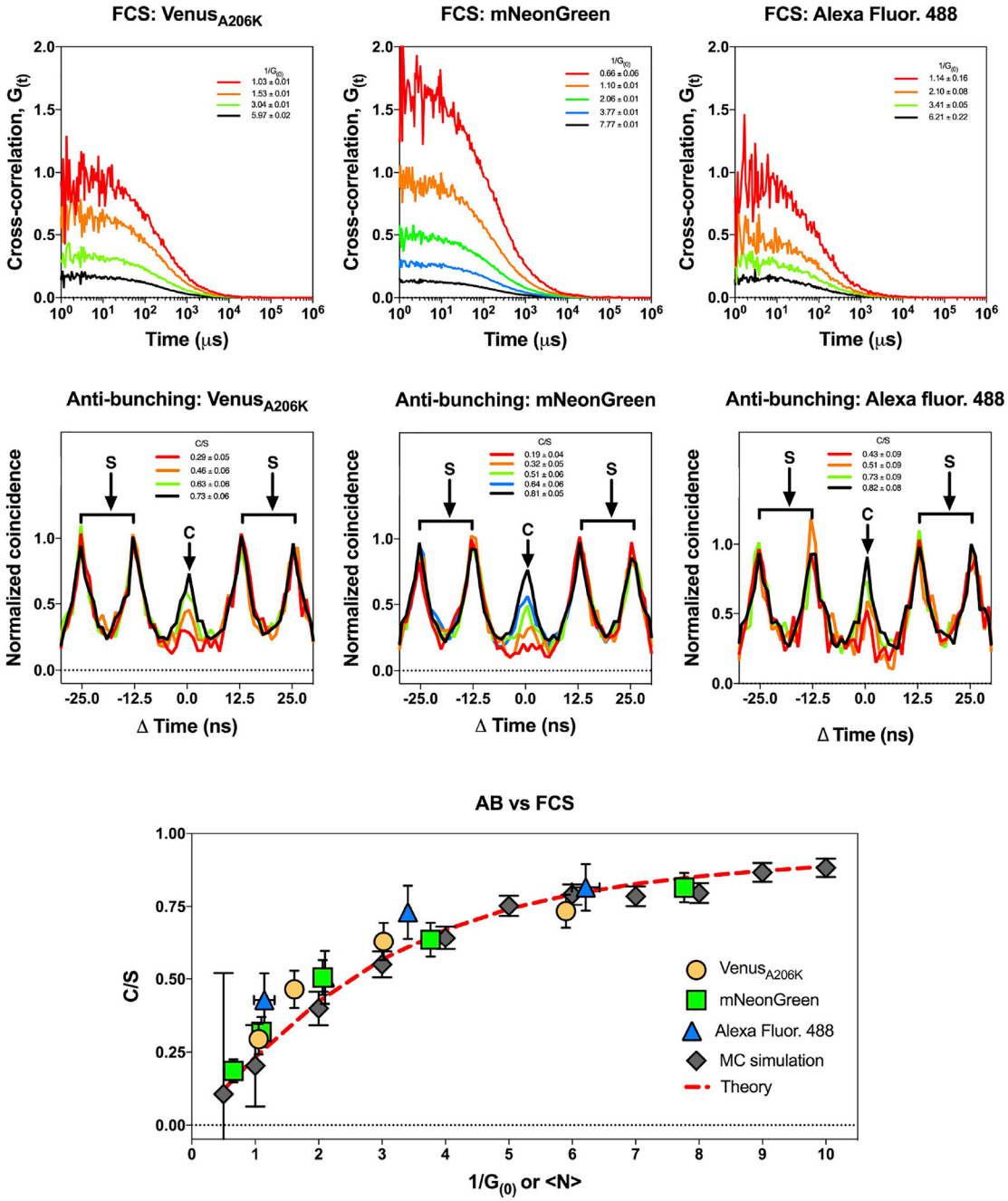

FIGURE 4 Validating AB/FCS fingerprinting. FCS (*top row*) and antibunching (*center row*) were performed for dilutions of Venus$_{A206K}$ (*left*), mNeonGreen (*center*), and Alexa Fluor 488 (*right*). The center peak of antibunching curves is depicted as C, and the four side peaks are depicted as S to illustrate how C/S ratios are calculated. C/S ratios were plotted as a function of $1/G_{(0)}$ (*bottom panel*). For comparison, data generated by Monte Carlo simulation for antibunching C/S ratios from a single-photon emitter in solution as a function of the average number of molecules in the observation volume were generated and plotted (*gray diamonds*). The predicted antibunching theory for monomeric fluorophores in solution using the zero-truncated Poisson distribution is plotted as a red dashed line. Error bars indicate the SD of C/S and $1/G_{(0)}$ values derived from fitting antibunching and FCS data, respectively.

emitters in a sample (21,22,61). Photon AB is predicated on the idea that a single quantum entity can only emit one photon at a time and that photons are quantal. Thus, if the emission from a single fluorophore is split into two paths, the photons detected in each path should be anticorrelated (sub-Poissonian) on a timescale that is less than the lifetime of the fluorophore. In other words, few, if any, coincident photons should be detected as Δ time approaches zero. In contrast, because a single fluorophore can emit photons with multiple rounds of excitation and emission, on a

timescale longer than its fluorescence lifetime (i.e., at Δ time equals ± 12.5 or ± 25 ns for Venus using an 80 MHz pulsed laser for excitation), coincident photons should be readily detected with similar probabilities. The ratio of coincidence detection at Δ time zero (called the center peak) divided by the number of coincidences detected at side peaks (i.e., at Δ time equals ± 12.5 and ± 25 ns) is called the center-to-side (C/S) ratio and is proportional to the number of independent emitters in a sample. The lower the C/S ratio, the fewer independent emitters are present in the observation volume. By definition, a monomeric fluorophore is a single quantum emitter. Thus, a plot of AB (C/S) versus $1/G_{(0)}$ for dilutions of any monomeric fluorophore should yield the same "AB fingerprint," which is the number of independent emitters as a function of the average number of fluorescent molecules in the excitation volume. We validated AB/FCS fingerprinting by measuring serial dilutions of $Venus_{A206K}$, mNeonGreen (62), and Alexa Fluor 488 (Molecular Probes, Eugene, OR) (Fig. 4, *bottom*). All were in good agreement with AB Monte Carlo simulations for a single quantum emitter (when $\chi_\gamma = 1$) and with predicted AB theory for monomeric fluorophores in solution using the ZTP distribution.

Because AB and FCS are most effective when only a few fluorophores populate the observation volume, AB/FCS fingerprinting at the concentrations required for $Venus_{A206}$ dimerization is problematic. To overcome this limitation, we engineered a $Venus_{A206}$ tandem dimer ($Venus_{A206}$-TD). Even at low concentrations, its effective Venus concentration should promote A206 mediated dimerization. As expected, a dramatic reduction in anisotropy was observed (Fig. 5 *A*) with a limiting anisotropy of 0.20 at 0.5 μM, comparable to the limiting anisotropy of $Venus_{A206}$ at 740 μM. For comparison, monomeric $Venus_{A206K}$ had a limiting anisotropy of 0.42 at 0.7 μM. We also engineered a $Venus_{A206K}$ tandem dimer with the Venus fluorophores separated by a 20 nm linker (30) ($Venus_{A206K}$-20nm-TD). This construct had a limiting anisotropy of 0.42 at 0.9 μM, suggesting little, if any, ET. Brightness analysis confirmed that $Venus_{A206}$-TD was 2.0 $\pm$ 0.1 (mean $\pm$ SD) times as bright as a Venus monomer, and $Venus_{A206K}$-20nm-TD was 1.8 $\pm$ 0.1 times as bright (Fig. 5 *B*). Both of these values were statistically higher than the monomer ($p < 0.0001$, by analysis of variance), confirming that both constructs have two fluorophores.

AB spectroscopy of monomeric $Venus_{A206K}$ and $Venus_{A206}$-TD revealed an attenuated center coincidence peak (at comparable $1/G_{(0)}$ values, Fig. 5 *C*) with indistinguishable C/S ratios (0.19 $\pm$ 0.04 and 0.20 $\pm$ 0.03); these samples display strong and comparable AB. In contrast, $Venus_{A206K}$-20nm-TD had an elevated C/S ratio (0.36 $\pm$ 0.07). If $Venus_{A206K}$-20nm-TD fluorophores act independently, the $Venus_{A206K}$-20nm-TD fingerprint should systematically shift to higher C/S values than $Venus_{A206K}$ or $Venus_{A206}$-TD. As predicted, this was observed (Fig. 5 *D*). Theoretically, constructs with two independent emitters should always have C/S values $\geqq 0.5$. Surprisingly, the $Venus_{A206K}$-20nm-TD sample had an asymptote below 0.4. This anomaly, as well as its reduced normalized brightness (1.8, Fig. 5 *B*), suggests that this sample was comprised primarily of $Venus_{A206K}$-20nm-TD, along with some monomeric degradation products. Because only a single point from the $Venus_{A206}$-TD AB/FCS fingerprint clearly differed from the $Venus_{A206K}$ monomer,

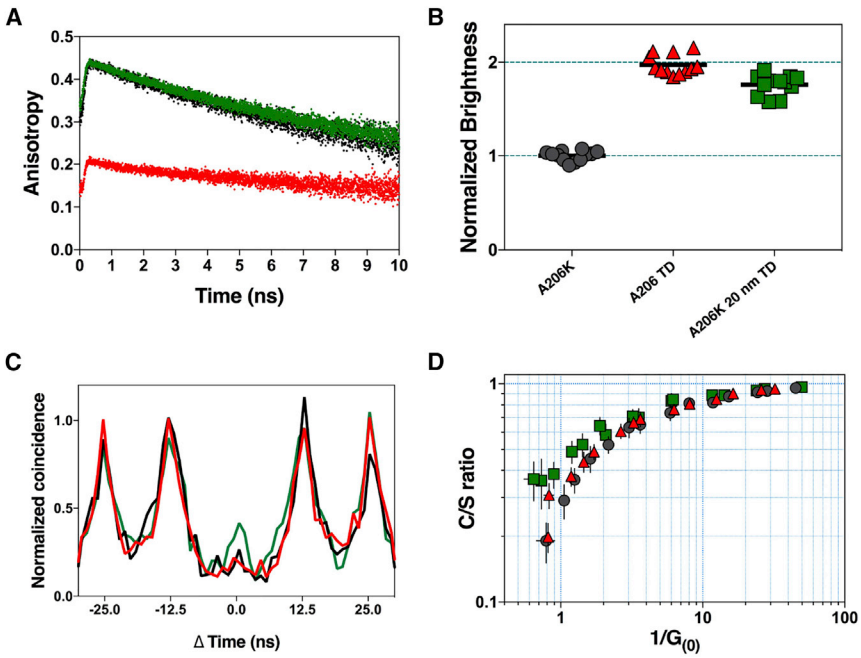

FIGURE 5 The $Venus_{A206}$-TD behaves as a single-photon emitter. (*A*) TRFA of $Venus_{A206K}$ (*black*), $Venus_{A206}$-TD (*red*), and $Venus_{A206K}$-20nm-TD (*green*) are shown. (*B*) The brightness of $Venus_{A206}$-TD (*red triangles*) and $Venus_{A206K}$-20nm-TD (*green squares*) were normalized to the brightness of $Venus_{A206K}$ monomers (*black circles*). Bars indicate the mean (n = 12) from three preparations (four replicates each). Dashed lines indicate the expected normalized brightness for monomers and dimers. (*C*) Shown are normalized photon antibunching traces for monomeric $Venus_{A206K}$ (*black*), dimeric $Venus_{A206}$-TD (*red*), and dimeric $Venus_{A206K}$-20nm-TD (*green*) at a $1/G_{(0)}$ values of 0.79 $\pm$ 0.11, 0.82 $\pm$ 0.02, and 0.65 $\pm$ 0.10, respectively. (*D*) Shown is the AB/FCS fingerprinting of monomeric $Venus_{A206}$ (*gray circles*), dimeric $Venus_{A206}$-TD (*red triangles*), and dimeric $Venus_{A206K}$-20nm-TD (*green squares*). *X*- and *Y*-axis error bars indicate the SD of C/S & $1/G_{(0)}$ measurements derived from fitting antibunching and FCS data, respectively.

we conclude that this dimer acts as a single-photon emitter.

An alternative explanation for strong AB could be that singlet-singlet annihilation reduces two excitation events to one emission event (22). Because annihilation is dependent on excitation power (63), we investigated if increasing excitation power altered $Venus_{A206}$-TD limiting anisotropy or, conversely, if decreasing power altered its AB/FCS fingerprint. In both cases, a dependence on excitation power was not observed (Fig. 6, *A* and *B*), arguing against an annihilation mechanism.

DISCUSSION

It is remarkable that at room temperature, a $Venus_{A206}$ dimer, an assembly composed of ~9000 atoms, displays two expected behaviors associated with CET, ultrafast ET and Davydov splitting. ET between $Venus_{A206}$ molecules in a dimer manifested as a drop in the limiting anisotropy. Because ET measurements in this study were limited by the instrument response function of our time-resolved anisotropy system, ~146 ps, we can conclude that ET between $Venus_{A206}$ fluorophores is faster than 146 ps. Because $Venus_{A206}$ and YFP_{A206} are almost identical structurally, it is likely that the rate of ET between $Venus_{A206}$ dimers is similar to the rate observed between YFP dimers (4.4 ps time constant) (16).

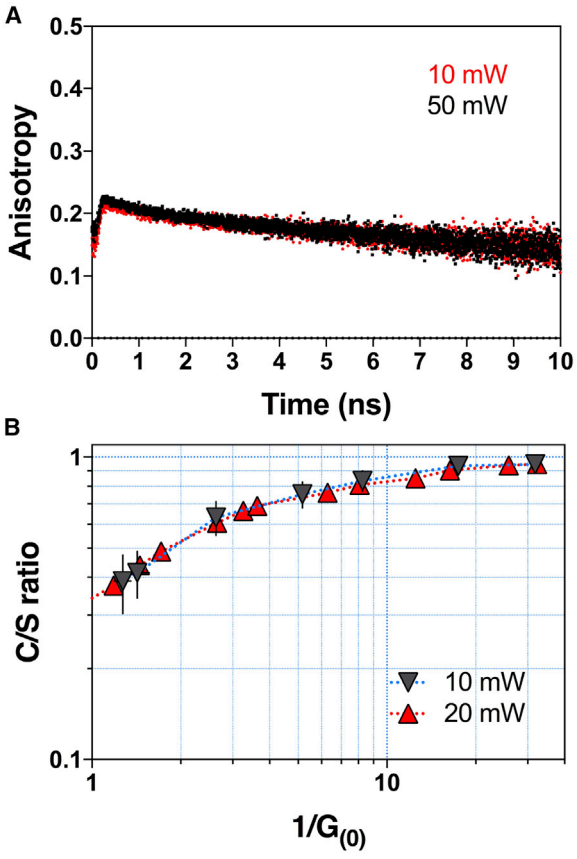

FIGURE 6 $Venus_{A206}$-TD ultrafast ET and antibunching are independent of excitation power. (*A*) Shown is the TRFA of $Venus_{A206}$-TD using either 10 mW (*red*) or 50 mW (*black*) two-photon excitation (power measured at the objective). (*B*) Shown is the AB/FCS fingerprinting of $Venus_{A206}$-TD using 10 mW two-photon excitation (*gray inverted triangles*). For comparison, the $Venus_{A206}$-TD AB/FCS fingerprint using 20 mW two-photon excitation (*red triangles*) from Fig. 5 *D* is replotted.

The observation of Davydov splitting in the $Venus_{A206}$ CD spectra when dimers form indicates the existence of a molecular exciton. Thus, we conclude that two Venus excited states can interact coherently at room temperature, presumably via intermediate-regime coupling. Because steady-state CD spectroscopy measures absorbance, an ultrafast process occurring on a 1–10 fs timescale, we do not know how long-lived the coherent interaction between $Venus_{A206}$ excited states persists. Nonetheless, we can use the formalism of Knox and Kenkre (6,10) to constrain our estimate for the rate of dephasing (decoherence) in a $Venus_{A206}$ dimer. In their formalism, if intermediate-regime coupling is observed, the dephasing rate of that sample should be within an order of magnitude of the samples' ET rate. Thus, if the transfer rate of $Venus_{A206}$ in a dimer is comparable to the measured $EYFP_{A206}$ ET rate (16), its dephasing time constant should be between 440 fs and 44 ps, in agreement with the 1 ps dephasing time measured for GFP (17).

$Venus_{A206}$-TD exhibited strong AB, indicating that its two fluorophores emit only a single photon in response to excitation. One explanation for this behavior is that when two independent Venus fluorophores in a $Venus_{A206}$-TD both absorb a photon, the two resulting excited states undergo high-efficiency singlet-singlet annihilation to yield only one surviving excited state. Thus, two excitation events can produce a single emitted photon. Because singlet-singlet annihilation should be dependent on excitation power (63), this explanation is unlikely as $Venus_{A206}$-TD AB in this study was excitation power independent. Furthermore, annihilation does not explain the presence of Davydov splitting in CD spectra nor the power independence of the ultrafast anisotropy decay component, and annihilation processes are rarely 100% efficient. An alternative explanation is that the two Venus fluorophores in the $Venus_{A206}$-TD comprise a single quantum entity as a result of intermediate-regime coherent coupling and can therefore only absorb (and emit) one photon at a time. This hypothesis is consistent with the strong AB observed in this construct and is consistent with the observed excitation power independence. This explanation is also consistent with our observation of Davydov splitting in $Venus_{A206}$ dimers and with the observation of an excitation power-independent ultrafast anisotropy decay component.

The coherent coupling we observe between $Venus_{A206}$ dimers might explain anomalous behaviors observed in other FP assemblies (17,22,54,64,65). Related observations in tetrameric DsRed (22,54,65) suggests that coherent

interactions are a common FP motif. Based on Knox and Kenkre's formalism (6), coherence can be promoted by slowing dephasing. We speculate that in addition to maintaining close fluorophore proximity and a permissive dipole orientation, the FP β-barrel functions to lessen decoherence by isolating embedded fluorophores from the dephasing influences of the thermal bath (66). This hypothesis is supported by our previous observation that Venus fluorescence is not attenuated by potent external collisional quenchers, such as acrylamide or potassium iodide (44), but measurements of the Venus dephasing time are needed to directly test this hypothesis.

If ET between other FPs can occur via both FRET (with very weak regime coupling) and CET (for intermediate-regime coupling), the use of FPs in biological ET studies must be re-evaluated. ET via FRET is typically limited to distances under 10 nm, whereas ET via CET is thought to be possible at distances as large as 100 nm (5). The distance dependence of FRET is inversely proportional to the sixth power of the separation between fluorophores, whereas the distance dependence of CET is thought to be inversely proportional to the third power of the separation for strong coupling (7,8) or to an inverse power between three and six for intermediate-regime coupling (6,10). Furthermore, the dependence of FRET on dipole orientation is dependent on the square of the dipole orientation factor (κ^2) (50), whereas CET should be dependent on κ. Similarly, the dependence of FRET on the refractive index is inversely proportional to the fourth power of refractive index (47,67), whereas CET should be inversely proportional to the second power. Finally, as we have shown for $\text{Venus}_{\text{A206}}$, intermediate-regime coupling can alter its absorbance spectrum. Thus, the overlap integral for ET might also change. Clearly, the calculation of distance based on ET data that assumes a FRET mechanism may be erroneous if the true underlying mechanism is CET or a mixture of CET and FRET.

At 2.5 nm separation, Dexter's electronic exchange should not occur between Venus fluorophores, and the dipole approximation for Coulombic coupling should be valid (9,11). Our study also indicates that covalent continuity between the two $\text{Venus}_{\text{A206}}$ molecules in a dimer is not required for their coherent behavior; thus, a through-bond mechanism for ET in this system is unlikely. Furthermore, because our CD experiments were performed using one-photon excitation and our AB and FCS experiments were performed using two-photon excitation, it is unlikely that $\text{Venus}_{\text{A206}}$ excited-state coherence is dependent on the path used for excitation. Because cryogenic temperatures are not required for the coherent behaviors observed, FP tandem dimers might form a basis for building low-cost quantum computers and single-photon sources and are an ideal preparation for studying intermediate-regime coupling and investigating how dephasing influences the coherence of ET (6).

SUPPORTING MATERIAL

Supporting Material can be found online at https://doi.org/10.1016/j.bpj.2019.04.014.

AUTHOR CONTRIBUTIONS

Y.K. designed and built AB instrumentation. Y.K. and T.A.N. designed and built anisotropy and FCS instrumentation. Y.K. and T.A.N. performed anisotropy and FCS measurements. Y.K. performed AB measurements. E.C. and D.S.K. performed CD and absorbance measurements. H.L.P. and G.H.T. produced reagents. H.L.P. purified reagents for CD analysis. Y.K., E.C., T.A.N., D.S.K., P.S.B., and S.S.V. analyzed data. S.S.V. wrote and performed AB Monte Carlo simulations. P.S.B. derived closed form solution for AB/FCS fingerprinting. S.S.V. designed the study and wrote the article with instrumental input from all coauthors.

ACKNOWLEDGMENTS

We thank K.M. Berland, R. Clegg, K. Suhling, E. Gratton, and V.M. Kenkre for stimulating discussions.

This work was funded by the intramural programs of the National Institutes of Health, National Institute on Alcohol Abuse and Alcoholism, and the Eunice Kennedy Shriver National Institute of Child Health and Development, Bethesda, MD 20892 and by National Institutes of Health S10OD016246-01A1 awarded to University of California, Santa Cruz.

REFERENCES

1. Chenu, A., and G. D. Scholes. 2015. Coherence in energy transfer and photosynthesis. *Annu. Rev. Phys. Chem.* 66:69–96.
2. Nelson, P. C. 2018. The role of quantum decoherence in FRET. *Biophys. J.* 115:167–172.
3. Duan, H. G., V. I. Prokhorenko, …, R. J. D. Miller. 2017. Nature does not rely on long-lived electronic quantum coherence for photosynthetic energy transfer. *Proc. Natl. Acad. Sci. USA.* 114:8493–8498.
4. Wilkins, D. M., and N. S. Dattani. 2015. Why quantum coherence is not important in the Fenna-Matthews-Olsen complex. *J. Chem. Theory Comput.* 11:3411–3419.
5. Clegg, R. M. 2006. The history of FRET: from conception through the labors of birth. *In* Reviews in Fluorescence. C. D. Geddes and J. R. Lakowicz, eds. Springer, pp. 1–45.
6. Knox, R. S., and V. M. Kenkre. 1974. Theory of fast and slow excitation transfer rates. *Phys. Rev. Lett.* 33:803–806.
7. Förster, T. 1965. Delocalized excitation and excitation transfer. *In* Modern Quantum Chemistry. Part III. O. Sinanoglu, ed. Academic Press, pp. 93–137.
8. Kasha, M. 1963. Energy transfer mechanisms and the molecular exciton model for molecular aggregates. *Radiat. Res.* 20:55–70.
9. Valeur, B., and M. N. Berberan-Santos. 2012. Molecular Fluorescence. Wiley-VCH, Weinheim, Germany.
10. Rahman, T. S., R. S. Knox, and V. M. Kenkre. 1979. Theory of Depolarization of fluorescence in molecular pairs. *Chem. Phys.* 44:197–211.
11. Andrews, D. L., C. Curutchet, and G. D. Scholes. 2011. Resonance energy transfer: beyond the limits. *Laser Photonics Rev.* 5:114–123.
12. Rekas, A., J. R. Alattia, …, M. Ikura. 2002. Crystal structure of venus, a yellow fluorescent protein with improved maturation and reduced environmental sensitivity. *J. Biol. Chem.* 277:50573–50578.
13. Nagai, T., K. Ibata, …, A. Miyawaki. 2002. A variant of yellow fluorescent protein with fast and efficient maturation for cell-biological applications. *Nat. Biotechnol.* 20:87–90.

14. Siegel, R. M., F. K. Chan, …, M. J. Lenardo. 2000. Measurement of molecular interactions in living cells by fluorescence resonance energy transfer between variants of the green fluorescent protein. *Sci. STKE.* 2000:pl1.

15. Stryer, L., and R. P. Haugland. 1967. Energy transfer: a spectroscopic ruler. *Proc. Natl. Acad. Sci. USA.* 58:719–726.

16. Jung, G., Y. Ma, …, G. R. Fleming. 2005. Ultrafast fluorescence depolarisation in the yellow fluorescent protein due to its dimerisation. *ChemPhysChem.* 6:1628–1632.

17. Cinelli, R. A., V. Tozzini, …, M. Giacca. 2001. Coherent dynamics of photoexcited green fluorescent proteins. *Phys. Rev. Lett.* 86:3439–3442.

18. Davydov, A. S. 1971. Theory of Molecular Excitons. Plenum Press, New York.

19. Grishina, I. B., and R. W. Woody. 1994. Contributions of tryptophan side chains to the circular dichroism of globular proteins: exciton couplets and coupled oscillators. *Faraday Discuss.* 99:245–262.

20. Tanaka, K., G. Pescitelli, …, N. Berova. 2005. Fluorescence detected exciton coupled circular dichroism: development of new fluorescent reporter groups for structural studies. *Monatsh. Chem.* 136:367–395.

21. Paul, H. 1982. Photon antibunching. *Rev. Mod. Phys.* 54:1061–1102.

22. Sánchez-Mosteiro, G., M. Koopman, …, M. F. García-Parajó. 2004. Photon antibunching proves emission from a single subunit in the autofluorescent protein DsRed. *ChemPhysChem.* 5:1782–1785.

23. Sýkora, J., K. Kaiser, …, J. Enderlein. 2007. Exploring fluorescence antibunching in solution to determine the stoichiometry of molecular complexes. *Anal. Chem.* 79:4040–4049.

24. Elson, E. L., and D. Madge. 1974. Fluorescence correlation spectroscopy. I. Conceptual basis and theory. *Biopolymers.* 13:1–27.

25. Magde, D., E. L. Elson, and W. W. Webb. 1974. Fluorescence correlation spectroscopy. II. An experimental realization. *Biopolymers.* 13:29–61.

26. Thompson, N. L. 1991. Fluorescence correlation spectroscopy. *In* Topics in Fluorescence Spectroscopy. J. R. Lakowicz, ed. Plenum Press, pp. 337–378.

27. Berland, K. M., P. T. So, and E. Gratton. 1995. Two-photon fluorescence correlation spectroscopy: method and application to the intracellular environment. *Biophys. J.* 68:694–701.

28. Schwille, P., J. Korlach, and W. W. Webb. 1999. Fluorescence correlation spectroscopy with single-molecule sensitivity on cell and model membranes. *Cytometry.* 36:176–182.

29. Cranfill, P. J., B. R. Sell, …, D. W. Piston. 2016. Quantitative assessment of fluorescent proteins. *Nat. Methods.* 13:557–562.

30. Sivaramakrishnan, S., and J. A. Spudich. 2011. Systematic control of protein interaction using a modular ER/K α-helix linker. *Proc. Natl. Acad. Sci. USA.* 108:20467–20472.

31. Thaler, C., S. V. Koushik, …, S. S. Vogel. 2009. Structural rearrangement of CaMKIIalpha catalytic domains encodes activation. *Proc. Natl. Acad. Sci. USA.* 106:6369–6374.

32. Vogel, S. S., C. Thaler, …, S. V. Koushik. 2010. Time resolved fluorescence anisotropy. *In* FLIM Microscopy in Biology and Medicine. A. Periasamy and R. M. Clegg, eds. Taylor & Francis, pp. 245–290.

33. Chandrasekhar, S. 1943. Stochastic problems in physics and astronomy. *Rev. Mod. Phys.* 15:1–89.

34. Müller, J. D., Y. Chen, and E. Gratton. 2003. Fluorescence correlation spectroscopy. *Methods Enzymol.* 361:69–92.

35. Nguyen, T. A., P. Sarkar, …, S. S. Vogel. 2012. Fluorescence polarization and fluctuation analysis monitors subunit proximity, stoichiometry, and protein complex hydrodynamics. *PLoS One.* 7:e38209.

36. Nguyen, T. A., P. Sarkar, …, S. S. Vogel. 2015. Covert changes in CaMKII holoenzyme structure identified for activation and subsequent interactions. *Biophys. J.* 108:2158–2170.

37. Sarkar, P., K. A. Davis, …, S. S. Vogel. 2017. Deciphering CaMKII multimerization using fluorescence correlation spectroscopy and homo-FRET analysis. *Biophys. J.* 112:1270–1281.

38. Nguyen, T. A., H. L. Puhl, III, …, S. S. Vogel. 2018. Auto-FPFA: an automated microscope for characterizing genetically encoded biosensors. *Sci. Rep.* 8:7374.

39. Nagy, A., J. Wu, and K. M. Berland. 2005. Observation volumes and gamma-factors in two-photon fluorescence fluctuation spectroscopy. *Biophys. J.* 89:2077–2090.

40. Hanbury Brown, R., and R. Q. Twiss. 1956. A test of a new type of stellar interferometer on sirius. *Nature.* 177:1046–1048.

41. Zacharias, D. A., J. D. Violin, …, R. Y. Tsien. 2002. Partitioning of lipid-modified monomeric GFPs into membrane microdomains of live cells. *Science.* 296:913–916.

42. Lidke, D. S., P. Nagy, …, T. M. Jovin. 2003. Imaging molecular interactions in cells by dynamic and static fluorescence anisotropy (rFLIM and emFRET). *Biochem. Soc. Trans.* 31:1020–1027.

43. Suhling, K., P. M. French, and D. Phillips. 2005. Time-resolved fluorescence microscopy. *Photochem. Photobiol. Sci.* 4:13–22.

44. Sarkar, P., S. V. Koushik, …, Z. Gryczynski. 2009. Photophysical properties of Cerulean and Venus fluorescent proteins. *J. Biomed. Opt.* 14:034047.

45. Periasamy, A., N. Mazumder, …, R. N. Day. 2015. FRET microscopy: basics, issues and advantages of FLIM-FRET imaging. Springer Series in Chemical Physics. Springer, p. 624.

46. Gadella, T. W. J., T. M. Jovin, and R. M. Clegg. 1993. Fluorescence lifetime imaging microscopy (FLIM): spacial resolution of microstructures on the nanosecond time scale. *Biophys. Chem.* 48:221–239.

47. Medintz, I., and N. Hildebrandt. 2013. FRET – Förster Resonance Energy Transfer. Wiley-VCH Verlag GmbH & Co. KGaA, Weinheim, Germany.

48. Kremers, G. J., and J. Goedhart. 2009. Visible fluorescent proteins for FRET. *In* FRET and FLIM Techniques. T. W. J. Gadela, ed. Elsevier, pp. 171–223.

49. van der Meer, B. W. 2002. Kappa-squared: from nuisance to new sense. *J. Biotechnol.* 82:181–196.

50. van der Meer, B. W., D. M. van der Meer, and S. S. Vogel. 2013. Optimizing the orientation factor kappa-squared for more accurate FRET measurements. FRET – Förster Resonance Energy Transfer. Wiley-VCH Verlag GmbH & Co. KGaA, pp. 63–104.

51. Vogel, S. S., T. A. Nguyen, …, P. S. Blank. 2012. The impact of heterogeneity and dark acceptor states on FRET: implications for using fluorescent protein donors and acceptors. *PLoS One.* 7:e49593.

52. Axelrod, D. 1979. Carbocyanine dye orientation in red cell membrane studied by microscopic fluorescence polarization. *Biophys. J.* 26:557–573.

53. Axelrod, D. 1989. Fluorescence polarization microscopy. *Methods Cell Biol.* 30:333–352.

54. Visser, N. V., M. A. Hink, …, A. J. Visser. 2002. Circular dichroism spectroscopy of fluorescent proteins. *FEBS Lett.* 521:31–35.

55. Schwille, P., U. Haupts, …, W. W. Webb. 1999. Molecular dynamics in living cells observed by fluorescence correlation spectroscopy with one- and two-photon excitation. *Biophys. J.* 77:2251–2265.

56. Elson, E. L., and W. W. Webb. 1975. Concentration correlation spectroscopy: a new biophysical probe based on occupation number fluctuations. *Annu. Rev. Biophys. Bioeng.* 4:311–334.

57. Berland, K. M., P. T. So, …, E. Gratton. 1996. Scanning two-photon fluctuation correlation spectroscopy: particle counting measurements for detection of molecular aggregation. *Biophys. J.* 71:410–420.

58. Schwille, P., S. Kummer, …, W. W. Webb. 2000. Fluorescence correlation spectroscopy reveals fast optical excitation-driven intramolecular dynamics of yellow fluorescent proteins. *Proc. Natl. Acad. Sci. USA.* 97:151–156.

59. Schwille, P. 2001. Fluorescence correlation spectroscopy and its potential for intracellular applications. *Cell Biochem. Biophys.* 34:383–408.

60. Chen, Y., J. D. Müller, …, E. Gratton. 1999. Fluorescence fluctuation spectroscopy. *Methods.* 19:234–252.

61. Kimble, H. J., M. Dagenais, and L. Mandel. 1977. Photon antibunching in resonance fluorescence. *Phys. Rev. Lett.* 39:691–695.

62. Shaner, N. C., G. G. Lambert, …, J. Wang. 2013. A bright monomeric green fluorescent protein derived from Branchiostoma lanceolatum. *Nat. Methods.* 10:407–409.

63. Fückel, B., G. Hinze, …, T. Basché. 2010. Quantification of the singlet-singlet annihilation times of individual bichromophoric molecules by photon coincidence measurements. *J. Phys. Chem. A.* 114:7671–7676.

64. Koushik, S. V., P. S. Blank, and S. S. Vogel. 2009. Anomalous surplus energy transfer observed with multiple FRET acceptors. *PLoS One.* 4:e8031.

65. Lounis, B., J. Deich, …, W. E. Moerner. 2001. Photophysics of DsRed, a red fluorescent protein, from the ensemble to the single-molecule level. *J. Phys. Chem. B.* 105:5048–5054.

66. Gilmore, J., and R. H. McKinzie. 2005. Spin boson models for quantum decoherence of electronic excitations of biomolecules and quantum dots in a solvent. *J. Phys. Condens. Matter.* 17:1735–1746.

67. Gadela, T. W. J. 2009. FRET and FLIM Techniques. Elsevier, Amsterdam, the Netherlands.